

Analysis of Averaging Methods for Nonuniform Total Pressure Fields

Daniel Burdett

Department of Engineering Science,
University of Oxford,
Oxford OX2 0ES, UK
e-mail: daniel.burdett@univ.ox.ac.uk

Thomas Povey¹

Department of Engineering Science,
University of Oxford,
Oxford OX2 0ES, UK
e-mail: thomas.povey@eng.ox.ac.uk

A common objective in the analysis of turbomachinery components (nozzle guide vanes (NGVs) or rotor blades, for example) is to calculate performance parameters, such as total pressure or kinetic energy (KE) loss coefficients, from measurements in a nonuniform flow-field. These performance parameters can be represented in a range of ways. For example, line-averages used to compare performance between different radial sections of a 3D component; plane-averages used to assess flow (perhaps loss coefficient) development between different axial planes; and fully mixed-out values used to determine the total loss associated with a component. In the literature, the weighting method used for line- and plane-averaging (e.g., area, volume flow, mass flow, or entropy-flux) is sometimes regarded as an unimportant issue. Indeed, many authors neglect to even state which weighting method was used in their work. In certain low-speed test cases, or where measurements are made a long distance from the component, the nonuniformity in the flow will be relatively small and the practical difference between different weighting methods may be negligible. However, in high-speed applications or for measurements close to a component trailing edge, this becomes increasingly unlikely. In this paper, we compare a range of methods for calculating aerodynamic performance parameters—for example, the kinetic energy loss coefficient—including plane-average methods with different weighting schemes and several mixed-out methods. We analyze the sensitivities of the different methods to the axial location of the measurement plane, the radial averaging range, and the exit Mach number. We use high-fidelity experimental data taken in several axial planes downstream of a cascade of engine parts: high-pressure (HP) turbine NGVs operating at transonic Mach number. The experimental data are complemented by computational fluid dynamics (CFD). We discuss the underlying physical mechanisms which give rise to the observed sensitivities. The objective is to provide guidance on the accuracy of each method in a relevant, practical application. [DOI: 10.1115/1.4053020]

Keywords: boundary layer development, computational fluid dynamics (CFD), fluid dynamics and heat transfer phenomena in compressor and turbine components of gas turbine engines, measurement techniques, turbomachinery blading design, wind turbine aerodynamic design

Introduction

The flow-field downstream of a turbomachine blade row is—to first order—two-dimensional, but often with significant three-dimensional secondary features. For the purpose of basic performance assessment and comparison, simplified performance parameters are commonly used. Two of the most common performance parameters are the total pressure loss coefficient, Y , and the kinetic energy (KE) loss coefficient, ζ . The relative merits of these two metrics are considered later. Whichever performance parameter is preferred, however, there remain numerous questions about how to represent said parameter. In particular, the following questions arise

- (1) Do we wish to represent the performance parameter as a local value (at a point in a plane), a line-averaged value (to represent a circumferential or radial variation), a plane-averaged value (as a single numerical representation of the efficiency), or a *mixed-out* value at a hypothetical downstream plane?
- (2) In a line or plane-averaging process, should the integral be weighted by area, volume-flux, mass-flux, or entropy-flux?

- (3) In a *mixing process*, should the flow: be mixed to an entirely uniform static pressure defined at a single, swirl-averaged radius [1]; be mixed at every radius to a circumferentially uniform static pressure, producing a radial profile [2] not necessarily satisfying a radial equilibrium condition; or be mixed to a pre-specified radial static pressure condition defined by a free or forced vortex (which does satisfy radial equilibrium)?

A tree of possible representations of a given performance metric is represented by Fig. 1. For each performance parameter (e.g., Y or ζ) this leads to 13 distinct methods of representing the variable. In this paper, we compare and discuss these representations using both experimental and computational data, in particular considering the sensitivity to the weighting and averaging processes. These different representations of a loss parameter, are, of course, suited to different analysis objectives. For example:

- Local distributions allow identification of specific loss structures within a flow-field, and detailed local flow comparisons between different experiments or between experiment and computational fluid dynamics (CFD).
- Line-averages are useful for analyzing wake characteristics (depth and thickness) and mixing rates.
- Plane-averages are useful for analyzing overall mixing rates and as a simple method for analyzing total loss.

¹Corresponding author.

Contributed by the Heat Transfer Division of ASME for publication in the JOURNAL OF TURBOMACHINERY. Manuscript received December 1, 2020; final manuscript received August 11, 2021; published online January 28, 2022. Assoc. Editor: Tom Verstraete.

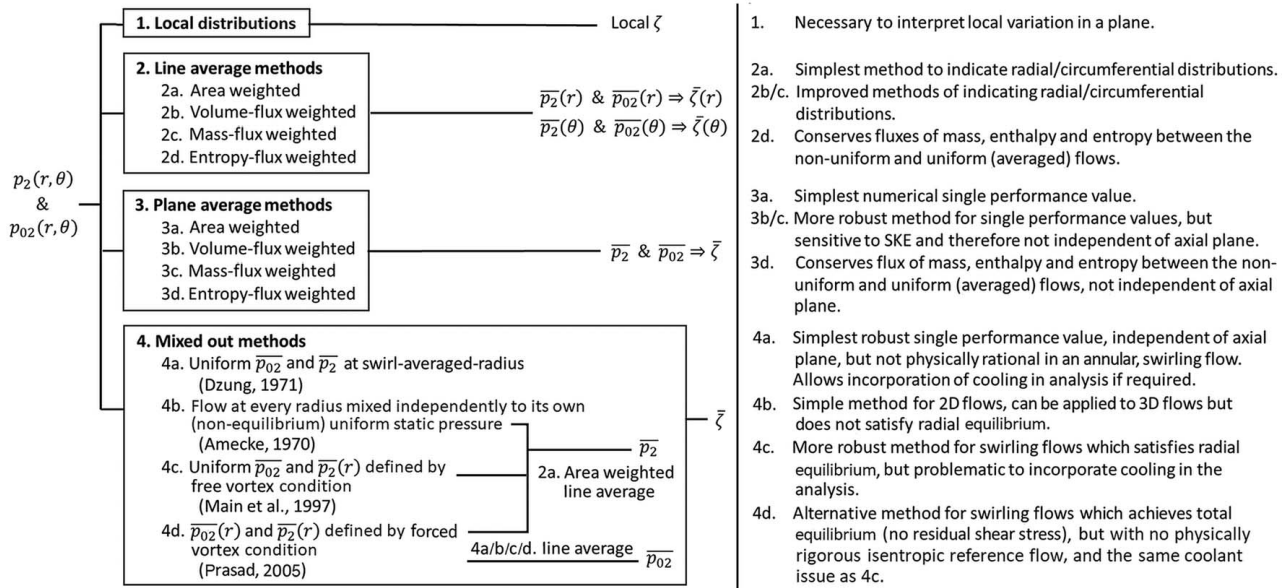


Fig. 1 Tree of possible performance metric calculations

- Mixed-out values are perhaps the most robust method for representing the total (plane-independent) loss associated with a component.

In many experiments in the open literature where averaged quantities are presented, a simple area-average is used, either because of the ease of calculation or because of difficulty in measuring the additional flow variables required for more sophisticated weighting methods. While simplicity is clearly desirable, it is important to consider the sensitivity (to axial plane, Mach number, etc.) that the choice of weighting method might imply. This is particularly important where comparing between different experiments, or between experiment and CFD.

In this paper, we examine the sensitivity of average loss representations to weighting method for the case of line-averaged and plane-averaged flows, and the sensitivity to mixing method for the case of mixed-out flows. We explain how differences between the methods arise (through examination of the nonuniform static pressure field), consider the sensitivity of the results to exit Mach number, and discuss the physical interpretation of the various representations of a performance parameter. We use experimental data from a transonic annular engine-parts facility, acquired at very

high spatial resolution in several axial planes, alongside complementary CFD data.

History of Total Pressure Performance Parameters, Averaging, and Mixing Methods

It is generally accepted that averaging of total temperature should be done using a mass-flux-weighted average. For a perfect gas (i.e., $h_0 = c_p T_0$), this conserves total enthalpy flux between the measured nonuniform and equivalent (hypothetical) uniform flows and is required in order to satisfy the first law of thermodynamics [3–5].

In contrast, there is neither complete consensus regarding the most appropriate performance parameter to represent total pressure loss, nor the best way to calculate an average of that parameter. Some of this divergence may arise from misunderstanding about best practice, while in other cases it could be argued that it is the result of reasonable compromises having been made (prioritizing practicality over rigor).

Review of Performance Parameters. Arguably the two most commonly used total pressure performance parameters (see, for example, Denton [6]) are the total pressure loss coefficient, Y , and the KE loss coefficient, ζ . We define Y for a turbine NGV or stage as

$$Y = \frac{p_{01} - p_{02}}{p_{01} - p_2} \quad (1)$$

where p_{01} , p_{02} , and p_2 are the row inlet total pressure, row exit total pressure, and row exit static pressure, respectively. The denominator is therefore the ideal row exit dynamic pressure. A weakness of this variable is that in a compressible flow, the denominator is not directly proportional to the exit kinetic energy ($p_0 - p \neq 0.5\rho v^2$). If the primary purpose of the nozzle is taken to be the conversion of potential (pressure) energy to outgoing angular momentum flux, the nonlinearity of definition (1) at compressible Mach numbers makes this variable problematic. The KE loss coefficient does not suffer from this problem because it can be related to the energy conversion efficiency, η , at all Mach numbers. We define η as

$$\eta = \frac{\text{Actual exit KE}}{\text{Ideal exit KE}} = \frac{v_2^2}{v_{2s}^2} = \frac{h_{02} - h_2}{h_{01} - h_{2s}} \quad (2)$$

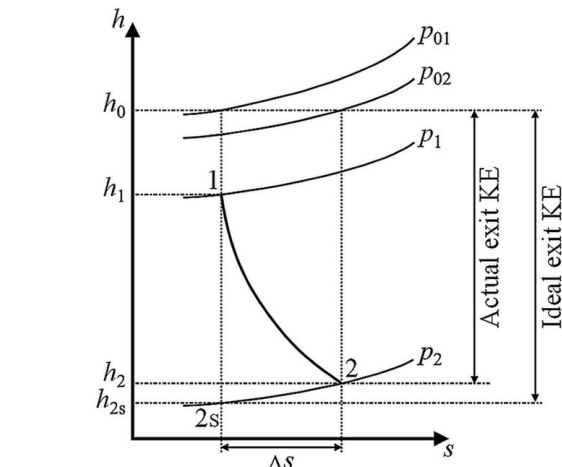


Fig. 2 h - s chart showing the simplified turbine expansion process

where v_2 and v_{2s} are the actual (measured) and isentropic exit velocities, respectively. For an adiabatic nozzle, $h_{02} = h_{01} = h_0$. The simplified expansion process is shown in the h - s chart in Fig. 2.

Defining the corresponding KE loss coefficient as $\zeta = 1 - \eta$, and using the isentropic relation $T_2/T_1 = (p_2/p_1)^{\chi}$ where $\chi = (\gamma - 1)/\gamma$, the loss coefficient becomes

$$\zeta = 1 - \frac{1 - \frac{h_2}{h_0}}{1 - \frac{h_{2s}}{h_0}} = 1 - \frac{1 - \left(\frac{p_2}{p_{02}}\right)^{\chi}}{1 - \left(\frac{p_2}{p_{01}}\right)^{\chi}} \quad (3)$$

In this paper, we primarily use ζ as the measure of NGV loss, and reference Y only to compare the sensitivities of the two parameters. For completeness, we note here that in the incompressible case, where $p_{02} - p_2 = 0.5\rho v_2^2$, ζ , and Y converge to the same numerical value.

Review of Averaging Methods. Pianko and Wazelt [3] presented a comprehensive review of the methods in common use for averaging nonuniform internal flows in turbomachines. They concluded that it is not possible to replace a real, nonuniform flow with an equivalent uniform (i.e., averaged) flow matching all significant fluxes and parameters. The significant literature is in agreement on this point [5,7].

Oates [4] discussed common methods for averaging nonuniform total pressure. For the simple case of two jets of different total pressure mixing adiabatically in a frictionless, constant-area duct, he showed that three different averaging methods produced average total pressure results with three different sensitivities to axial mixing distance: *mass-averaged* total pressure decreased with mixing distance (due to mixing out of secondary kinetic energy (SKE)); *stream-thrust-averaged* total pressure (in which the flow is fully mixed to a uniform condition) was insensitive to mixing distance; and *continuity-averaged* total pressure (calculated from a measured duct area, mass flowrate, static pressure, and total temperature by assuming the flow to be uniform over the whole area—sometimes used in situations where the conditions of individual constituent flows are known, but direct traverse probe access to the mixed flow is not possible) increased with mixing distance.

Cumpsty and Horlock [5] propose that the “correct” method for averaging total pressure in a nonuniform field is that which ensures that the property of interest in a particular application (e.g., work input/output, thrust, capacity, etc.) has the same value in the averaged flow and the real (nonuniform) flow. In particular, they discuss some common applications in turbomachinery flows: nonuniform flow entering a compressor or turbine (in which the work input or output is the important parameter); nonuniform flow entering a propelling nozzle (in which the gross thrust is the important parameter); and nonuniform flow entering a choked nozzle row (in which the flow capacity is the important parameter). They also note that, while there is no good physical basis for mass-averaging total pressure (flux-based averages such as the mass-flow-weighted average have no physical meaning when applied to intensive rather than extensive quantities), in many typical experimental situations the absolute variation in total pressure is sufficiently small that the difference between mass-averaging and more physically rigorous methods is small.

Review of Mixing Methods. The most commonly used methods for calculating the fully mixed-out total pressure in a nonuniform field are: mixing to a uniform static pressure defined at a single swirl-averaged radius (developed by Dzung [1]); uniform static pressure, proposed by Amecke [2]; and the free-vortex method of Main et al. [8]. The history of these three methods is reviewed by Main et al. [8]. For the case of an annular NGV cascade, a maximum disagreement in the evaluated efficiency between the three methods of 0.12% was demonstrated, across a range of pressure ratio conditions and downstream traverse plane locations.

Prasad [9] conducts a similar analysis to Main et al. [8], but enforces a *forced vortex*—rather than *free vortex*—at the hypothetical mixed-out plane. The loss coefficient calculated in this manner is found to be insensitive to the location of the plane in which the nonuniform data are taken. There are advantages and drawbacks of both the mixed-out conditions (free or forced vortex). A forced vortex is the only possible swirling, annular flow that can be in complete kinematic (all elements of the strain rate tensor are zero) and thermal (flow supports no temperature gradients) equilibrium. However, the resulting mixed-out flow has a radial gradient of total pressure, $p_{02}(r)$, with higher total pressure at larger radii. This means it is not possible to define a reference isentropic forced-vortex condition (required to define a loss coefficient), in cases where the inlet total pressure, p_{01} , is radially uniform. In contrast, a free vortex has a nonzero component of the strain rate tensor and hence is not entirely self-sustaining, but mixes the flow to a uniform total pressure, p_{02} . The free-vortex method therefore does not suffer from the issue of defining a reference isentropic condition.

Definitions for Averaging and Mixing Methods

In this section, we define the calculation process for each of the possible performance metric representations in Fig. 1. The KE loss coefficient is used in these examples.

Local Loss Parameters. The KE loss coefficient can be presented as a function of r and θ as follows:

$$\zeta(r, \theta) = 1 - \frac{1 - \left(\frac{p_2(r, \theta)}{p_{02}(r, \theta)}\right)^{\chi}}{1 - \left(\frac{p_2(r, \theta)}{p_{01}}\right)^{\chi}} \quad (4)$$

where $p_2(r, \theta)$ and $p_{02}(r, \theta)$ are the static and total pressure distributions in the plane, and $\chi = (\gamma - 1)/\gamma$.

Line and Plane-Averaging Methods. There are three principal steps in a line-averaging or plane-averaging process:

- Calculation of area-average local static pressure.* The average static pressure is defined from the net force acting on the reference area [5]

$$F = \int p \, dA = \bar{p}A \quad (5)$$

where \bar{p} is the area-average static pressure. That area-averaging is the appropriate method for averaging static pressure is generally accepted and is not debated in this paper. The plane-average of p_2 , defined over a specific radial ($r_1 \leq r \leq r_2$) and circumferential ($\theta_1 \leq \theta \leq \theta_2$) range is

$$\overline{p_{2,A}} = \frac{\int_{\theta_1}^{\theta_2} \int_{r_1}^{r_2} p_2(r, \theta) r dr d\theta}{\int_{\theta_1}^{\theta_2} \int_{r_1}^{r_2} r dr d\theta} \quad (6)$$

The corresponding line-averages (e.g., at constant r or θ) are calculated by integrating only in one dimension.

- Calculation of average local total pressure.* Total pressure can be averaged using the chosen weighting method (methods 2a–d in Fig. 1), by integrating the product of local total pressure and the local value of the weighting variable, and dividing by the integral of the weighting variable. For each of area-weighting, volume-flow-weighting, mass-flow-weighting, and entropy-flux-

weighting, we get

$$\overline{p_{02,A}} = \frac{\int_{\theta_1}^{\theta_2} \int_{r_1}^{r_2} p_{02}(r, \theta) r dr d\theta}{\int_{\theta_1}^{\theta_2} \int_{r_1}^{r_2} r dr d\theta} \quad (7)$$

$$\overline{p_{02,V}} = \frac{\int_{\theta_1}^{\theta_2} \int_{r_1}^{r_2} p_{02}(r, \theta) v_x(r, \theta) r dr d\theta}{\int_{\theta_1}^{\theta_2} \int_{r_1}^{r_2} v_x(r, \theta) r dr d\theta} \quad (8)$$

where v_x is the magnitude of the velocity component normal to the integration plane

$$\overline{p_{02,M}} = \frac{\int_{\theta_1}^{\theta_2} \int_{r_1}^{r_2} p_{02}(r, \theta) \rho(r, \theta) v_x(r, \theta) r dr d\theta}{\int_{\theta_1}^{\theta_2} \int_{r_1}^{r_2} \rho(r, \theta) v_x(r, \theta) r dr d\theta} \quad (9)$$

and

$$\frac{\overline{p_{02,S}}}{p_{\text{ref}}} = \exp \left\{ \frac{\int_{\theta_1}^{\theta_2} \int_{r_1}^{r_2} \left[\ln \left(\frac{p_{02}(r, \theta)}{p_{\text{ref}}} \right) - \frac{\gamma}{\gamma-1} \ln \left(\frac{T_{02}(r, \theta)}{\overline{T_{01}}} \right) \right] d\dot{m}}{\int_{\theta_1}^{\theta_2} \int_{r_1}^{r_2} d\dot{m}} \right\} \quad (10)$$

where $\overline{T_{01}}$ and $T_{02}(r, \theta)$ are the mass-averaged inlet total temperature and the local distribution of total temperature in the measurement plane, respectively, p_{ref} is an arbitrary nonzero reference pressure, and $d\dot{m} = \rho(r, \theta) v_x(r, \theta) r dr d\theta$ represents a local element of mass flowrate (normal to the plane). The entropy-flux-weighted method is a line-averaging or plane-averaging method in which we choose to set the total entropy-flux of the averaged flow to the same value as the measured (nonuniform) flow at the same location (e.g., in the same axial plane). This might be considered desirable because the change in entropy-flux is the most direct measure of lost efficiency through the vane row. The method is applicable only to local line or plane-averaging processes and is not a mixed-out method: entropy-flux should not be conserved in a mixing process.

In the case of uniform total temperature ($T_{02}(r, \theta) = \overline{T_{01}} = T_0$), Eq. (10) simplifies to

$$\frac{\overline{p_{02,S}}}{p_{\text{ref}}} = \exp \left\{ \frac{\int_{\theta_1}^{\theta_2} \int_{r_1}^{r_2} \ln \left(\frac{p_{02}(r, \theta)}{p_{\text{ref}}} \right) d\dot{m}}{\int_{\theta_1}^{\theta_2} \int_{r_1}^{r_2} d\dot{m}} \right\} \quad (11)$$

That is, in the case of negligible total temperature variation, entropy-flux-weighted averaging is the same as mass-flow-averaging the natural logarithm of total pressure.

- (iii) *Calculation of average value of the performance parameter based on area-averaged static pressure and weighted-average total pressure (whichever weighting method used).* The average KE loss coefficient is expressed as

$$\bar{\zeta} = 1 - \frac{1 - \left(\frac{\overline{p_{2,A}}}{\overline{p_{02}}} \right)^{\frac{\gamma}{\gamma-1}}}{1 - \left(\frac{\overline{p_{2,A}}}{p_{01}} \right)^{\frac{\gamma}{\gamma-1}}} \quad (12)$$

where $\overline{p_{02}}$ is the weighted average total pressure, calculated by any one of the four methods outlined above. A similar process is followed for the average total pressure loss coefficient \bar{Y} .

Mixed-Out Averaging Methods. In mixed-out averaging methods, equations for conservation of mass, linear and angular momentum, and energy are solved between the nonuniform flow in the measurement plane, and a hypothetical fully

mixed-out plane. To close the equations, it is necessary to specify the static pressure distribution in the mixed-out flow. The way this is specified is the primary difference between different methods. The mixed-out averaging processes can be thought of as effectively including the residual SKE present in the measured nonuniform flow in the loss evaluation. The result is therefore less sensitive to the axial plane in which the data are measured. It could also be argued that the result is more relevant in situations where the SKE cannot be usefully recovered by the downstream machinery (as in most practical situations in compressors and turbines).

There are four mixed-out averaging methods in the literature:

- (1) Swirl-averaged mixing (method of Dzung [1]; see also Ref. [3]). Average quantities of the mixed-out flow (including total and static pressures) are computed at a single, swirl-averaged radius (that is, a nominal radius at which swirl velocity has its average value). This method is recommended for linear cascade flows, but in annular swirling flows the implied mixed-out flow cannot satisfy radial equilibrium.
- (2) Two-dimensional mixing (method of Amecke [2]; see also Ref. [10]). The flow is conceptually split up into a series of thin, radial layers of 2D flow, which are individually mixed out without interaction with neighboring layers. This gives a radial distribution of mixed-out flow parameters (including total and static pressures). The radial static pressure distribution would not necessarily satisfy a radial equilibrium condition due to the complete absence of radial mixing. An overall loss coefficient is evaluated from single total and static pressures obtained by integrating the radial distributions (usually the area-integral of static pressure and the mass-flow-integral of total pressure).
- (3) Free-vortex mixing (method of Main et al. [8]). The flow is mixed to a free-vortex condition; that is, the circumferential velocity component is constrained to be inversely proportional to radius. The mixed-out flow therefore has zero vorticity. The resultant mixed-out flow has uniform total pressure and a radial static pressure distribution which, unlike the other methods, does satisfy a radial equilibrium condition and is therefore closer to a physically realizable condition. This method has the drawback that in experiments it is problematic to include coolant flows in the definition of the ideal exit flow (for the purpose of defining a loss coefficient) unless the radial distribution of coolant input is known.
- (4) Forced-vortex mixing (method of Prasad [9]). The flow is mixed to a forced-vortex condition; that is, the circumferential velocity component is constrained to be linearly proportional to radius. The resultant mixed-out flow has nonzero vorticity and radial profiles of both static and total pressure (higher total pressure at higher radii). Unlike the free-vortex condition, this is a state of complete kinematic and thermal equilibrium (all shear stress components are zero). Like the free-vortex method, the inclusion of coolant flows in the loss coefficient definition is problematic.

Note on Order of Operations. In these calculations, it is the underlying physical variables (pressure, temperature, mass, etc.) which are averaged. The performance parameter is then defined using those average quantities. The question could arise: should we instead calculate the local distribution of a performance parameter, e.g., $\zeta(r, \theta)$, then perform a weighted average of the parameter. Although in practice—despite nonlinearity of the equations, e.g., (12)—the difference between the two process orders has minimal impact on the result, there is greater physical basis (control volume conservation arguments) for averaging the physical variables and this is therefore strongly preferred.

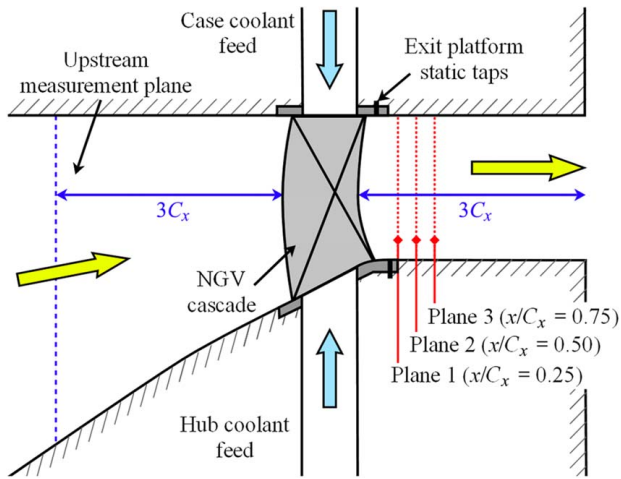


Fig. 3 Simplified diagram of an axisymmetric cross section through the ECAT facility working section

Table 1 Summary of nominal experimental test conditions

Variable	Nominal value
Inlet total pressure, p_{01}	2.00 bar
Inlet total temperature, T_{01}	290 K
Exit static pressure, p_2	1.10 bar
Mass flowrate, \dot{m}	14.0 kg/s
Inlet turbulence intensity, Tu	~8%
Coolant-to-mainstream pressure ratio, p_{0c}/p_{01}	1.025
Vane pressure ratio, p_2/p_{01}	0.550
Vane exit Mach number, M_2	0.965
Reynolds number, Re	1.3×10^6

Experimental Measurement Process

Experimental traverse measurements were performed in the Engine Component Aerothermal (ECAT) facility at the University of Oxford [11]. The ECAT facility is a high technology readiness level short-duration (approximately 60 s run time), blowdown facility currently built as an annular cascade of NGVs. A simplified axisymmetric schematic diagram is shown in Fig. 3. The NGVs are fully cooled parts from a modern civil engine, operating at conditions (Mach number, Reynolds number, coolant-to-mainstream pressure ratio) nondimensionally matched to the nominal engine operating point. The nominal operating conditions in ECAT tests are summarized in Table 1. The quoted Reynolds number is based on the vane tangential chord length and vane exit flow conditions. Inlet conditions of total pressure and temperature are measured at rakes located three axial chord lengths upstream of the cascade leading edge plane. A pressure regulator upstream of the working section maintains the inlet total pressure at steady state for the duration of the test. Vane exit static pressure is measured at a large number (approximately 100) of surface tappings located on the vane exit platforms at hub and case. The ratio of vane exit-static to inlet-total pressures defines the operating condition of the facility. Further details of these measurements and the associated uncertainties can be found in Refs. [12,13].

The vane cooling system includes approximately ten rows of surface films and coolant ejection from a trailing edge (TE) slot. Coolant is fed from cavities at both hub and case (see Fig. 3). The coolant feed mass flowrate is carefully controlled to achieve the target coolant-to-mainstream pressure ratio. The ECAT facility has previously been used to perform high-accuracy measurements of vane capacity [12–14], aerodynamic loss, and metal effectiveness [11].

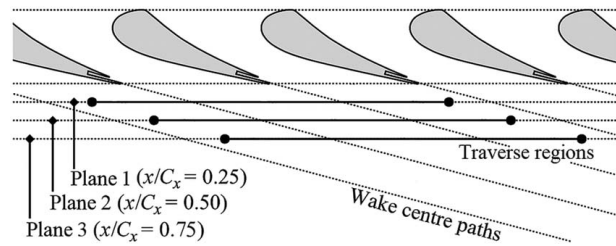


Fig. 4 Locations of the three experimental axial traverse planes

Traverse measurements were made downstream of the NGV cascade using an automated radial-circumferential traverse mechanism. Measurements were performed in three axial planes located 0.25, 0.50, and 0.75 axial chord lengths downstream of the cascade trailing edge plane. These axial planes are indicated in Fig. 4. Traverse measurements covered a circumferential range of 2.5 vane pitches. The traverse system was clocked in the circumferential direction between the axial planes so that wakes from the same vanes were measured at each axial position. A schematic is shown in Fig. 4. The radial traverse range was approximately 95% of vane span. In this range approximately 60 discrete circumferential passes of the traverse probe were performed at fixed radius. The average radial step height was approximately 1.4 mm. A typical complete area-survey traverse path is shown in Fig. 5. The complete path was made up of six separate experiments, represented by blocks in the figure. Adjacent blocks overlapped by at least one probe-pass to ensure consistency. Dashed black lines show the approximate locations of vane wakes.

The traverse probe used in this study was a five-hole pneumatic pressure probe with tip diameter 2.8 mm. The probe was calibrated over a range of flow Mach number $0.3 \leq M \leq 1.4$, and a range of incident flow angles (in two axes) of ± 40 deg. The traverse speed was set based on the estimated dynamic response of the probe-transducer system, such that the effective circumferential resolution was equivalent to half of the probe tip diameter (1.4 mm). This, in combination with the traverse pattern, gives an effective resolution of approximately 1.4 mm in both the radial and circumferential directions.

Numerical Method

3D Reynolds-averaged Navier–Stokes CFD simulations were performed using the commercial solver ANSYS CFX. The shear stress transport (SST) $k-\omega$ model was used for turbulence closure. The simulated geometry was an annular sector containing two vane pitches with rotational periodicity. The geometry is shown in Fig. 6(a). The vane geometries were taken from the design intent CAD drawing of the component tested in experiments,

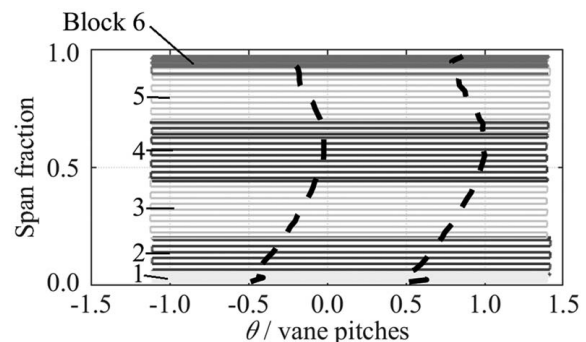


Fig. 5 Example traverse blocking arrangement for a single area-survey. Six separate tests are represented by the six blocks. Dashed lines show the wake locations.

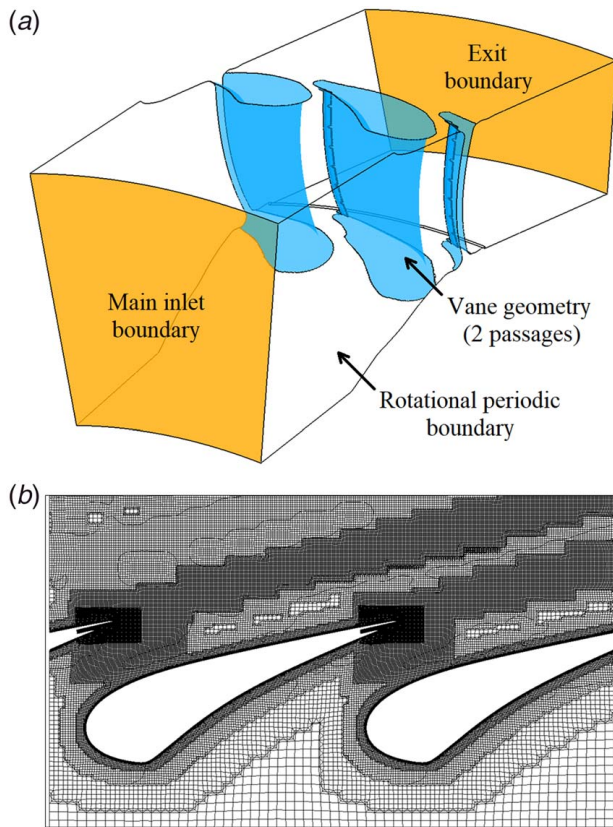


Fig. 6 (a) CFD geometry and (b) midspan mesh cross section

defeatured to remove film cooling holes from the vane surfaces. The domain was discretized with an Octree-based mesh using Boxer-Mesh. A cross section through the mesh at midspan is shown in Fig. 6(b). The mesh was refined close to the vane surfaces, in the vicinity of the trailing edges, and in the paths of the wakes downstream of the cascade. The final mesh size was approximately 57 million cells.

Boundary conditions were set to match the operating conditions achieved in experiments (Table 1). Uniform total pressure and temperature were imposed at the inlet plane. A target value of area-average static pressure was set on the exit boundary. The radial distribution of exit static pressure was additionally required to satisfy a radial equilibrium condition, while the circumferential static pressure distribution at any radial height was unconstrained. Static pressures were evaluated at the locations of the experimental pressure tapings on the hub and case vane exit platforms, and an iterative process (tuning the target value for area-average static pressure at the exit boundary) was used to match the exit-platform static-pressure-to-inlet-total-pressure ratio to the experimental value.

Film cooling flows were modeled using the *source term* method. A coolant mass flowrate (specified as a fraction of the mainstream mass flowrate) was applied at each film exit location. Details of the model for calculating mass flowrates for individual films can be found in Ref. [14]. The trailing edge coolant flow was set at an inlet boundary some distance (approximately eight slot widths) inside the trailing edge slot (to ensure proper flow development before issuing into the mainstream). A mass flow boundary condition was used. Further details of the trailing edge slot modeling can be found in Ref. [14].

Comparison of Averaging Methods

In this section, we compare the results of the various averaging methods using both experimental and numerical data. We first

introduce the nonuniform experimental and CFD flow fields. Figure 7 shows local distributions of KE loss coefficient, ζ (Eq. (4)), in three different axial planes, from experimental and numerical data, respectively.

Most importantly for our purpose, we have high spatial resolution in the experimental measurements, and similar general trends between CFD and experiment with well resolved wakes and secondary flow features. The under-predicted mixing rates in CFD simulations are a well-known problem and this is reflected in higher values of ζ in the wakes with respect to experiment (at a particular axial plane), and narrower wake profiles. The absolute KE (or total pressure) deficit associated with film cooling is also overestimated by the source terms model. Improved agreement with experiment would likely be achieved by fully resolving the geometry of all film cooling holes in the CFD model.

The radial pressure gradient, a characteristic feature of annular cascade flows, promotes migration of low-momentum flow toward the hub and away from the case. This generates intense secondary loss cores in the wake near the hub—also exacerbated by higher Mach numbers in this region—and lower intensity of secondary flows near the case. The radial profile of total pressure loss in the wake center over the vane span is also relatively well matched. The wake loss profile is broken up into a number of distinct sections separated by local minima in between. This effect is the result of internal cooling features within the trailing edge coolant slot. The wake regions decay in depth and broaden in width between the axial planes. The nonuniformity in the radial direction also gradually decays.

Although we describe the flow features for reference in later analysis, our primary purpose here is not good agreement between CFD and experiment, but rather a comprehensive dataset that shows typical differences between such results.

Plane-Average Weighting Functions. We now compare area-weighted, volume-flow-weighted, and mass-flow-weighted methods for plane-averaging total pressure. The weighting functions are the multipliers for total pressure in the numerators of Eqs. (7)–(9). We do not treat the entropy-flux-average separately because in the isothermal simplification (Eq. (11)) the method reduces to weighting the natural logarithm of total pressure using the mass-flow-weighting function. The weighting functions for the axial plane 1 are shown in Fig. 8, for both experimental data and CFD, normalized with respect to the maximum value in each case. Horizontal dashed lines indicate the radial limits used for the evaluation of the *profile* KE loss coefficient. We now consider the weighting functions in turn. To most clearly demonstrate the trends, the underlying (high-resolution) data are re-sampled onto a uniform grid in r and θ . The results presented are independent of this processing step, and raw data following the traverse pattern of Fig. 5 could equally be used (with associated radial distortions in the weighting functions).

The area-weighting functions (frames (a) in Fig. 8), have—trivially—a gradient in the radial direction on account of the uniform grid of data in r and θ .

The volume-flow-weighting functions (frames (b) in Fig. 8) have comparatively low weighting in the wake and film-mixing regions, associated with the low momentum in these areas. A strong radial pressure gradient from case to hub leads to slightly higher weighting at lower radii. The same effect can be seen with the cross-passage pressure gradient, with highest weighting near the vane suction side (SS), and lowest near the pressure side (PS).

The mass-flow-weighting functions (frames (c) in Fig. 8) are very similar to the volume-flow-weighting functions, but with small deviations associated with density variation.

To compare the weighting functions quantitatively, the values at midspan in planes 1, 2, and 3 are plotted as line functions in Fig. 9. The approximate locations of the wake centers are marked with dashed lines. Each trend is normalized with respect to its own

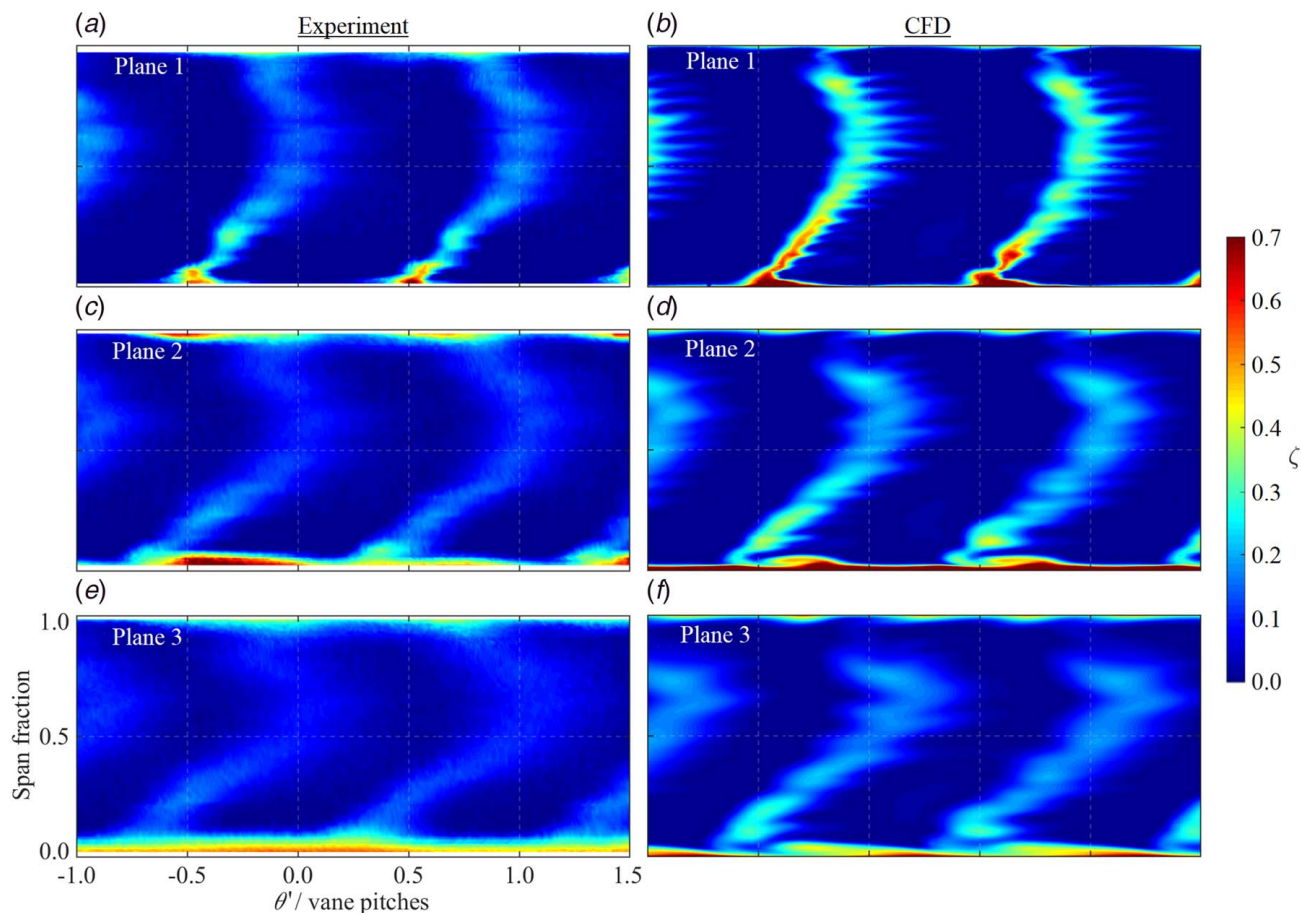


Fig. 7 Experimentally measured and CFD-predicted local distributions of kinetic energy loss coefficient, ζ , in the axial planes: (a)–(b) $x/C_x = 0.25$, (c)–(d) $x/C_x = 0.50$, and (e)–(f) $x/C_x = 0.75$

maximum value. In all cases, the area-weighting functions are constant at unity.

We now compare the volume flow and mass-flow-weighting functions. There is only a very slight difference moving between volume-flow-weighting and mass-flow-weighting, which results in biasing the average further in favor of the freestream regions (e.g., $0.4 \leq \theta \leq 0.6$) and against the wake regions (e.g., $-0.3 \leq \theta \leq 0.1$).

The general shape of the trends is very similar between CFD and experiment, but with significantly larger variation (from unity) for the experimental data compared with CFD. In the wake regions the experimental weighting functions have much deeper troughs than those for CFD (minimum values of normalized mass flow-weighting differ between experiment and CFD by 36.9%, 15.0%, and 16.2% in planes 1, 2, and 3, respectively), and the troughs are shifted toward the SS. This is surprising: given the more mixed-out local loss distributions observed in the experimental data compared with CFD in the equivalent plane (Fig. 7), we might have expected the opposite to be true. The differences can be explained by differences in exit whirl angle profiles, and total and static pressure fields between experiment and CFD. A comparison of whirl angle distributions at midspan between experiment and CFD is shown in Fig. 10, while static and total pressure fields are presented in Fig. 11.

Consider first the midspan whirl angle distributions in Fig. 10, where whirl angle, β , is defined as the angle between the local velocity vector and the axial direction, in the axial-circumferential plane. The profiles differ significantly between the three planes, becoming generally more mixed out with successive movements downstream. At a particular plane, the variation in angle in the experimental data is greater than the CFD predictions. For example, in plane 1, β varies circumferentially by 8.8 deg in the

experiment, and by only 2.9 deg in CFD. The under-prediction of whirl angle to the SS of the wake by CFD is thought to arise due to an exaggerated shock-boundary layer interaction, which causes the SS boundary layer to separate upstream of the trailing edge.

The larger whirl angle variation in the experimental data leads to greater circumferential variation in the axial velocity component, and therefore greater variation in the local volume flowrate and mass flowrate normal to the axial plane. This explains the deeper troughs in the normalized experimental weighting functions—see Fig. 9—which align with peaks (and associated lower local axial velocity) in the whirl angle distributions of Fig. 10.

To understand the difference in whirl angle distribution between the three planes, we now consider the total and static pressure fields in the exit flow. CFD-predicted midspan profiles of total and static pressure are presented in Figs. 11(a) and 11(b), respectively. Planes 1, 2, and 3 are marked in the figures by dashed black lines.

Looking first at the total pressure field (Fig. 11(a)), there are characteristic wakes which broaden in width and reduce in depth with distance in the streamwise direction. Even at plane 3, the wakes remain well-defined.

The static pressure (Fig. 11(b)) reduces through the covered part of the vane passage as the flow is accelerated. In the downstream flow between planes 1 and 3 (in the axial direction), the static pressure is relatively uniform over most of the domain, but with a significantly elevated region of pressure directly axially downstream of each trailing edge.

There are two interesting consequences of the interaction of the total and static pressure fields, which we now examine.

Firstly, we consider the development with axial distance of the whirl angle profiles shown in Fig. 10. In Fig. 12(a), we plot the

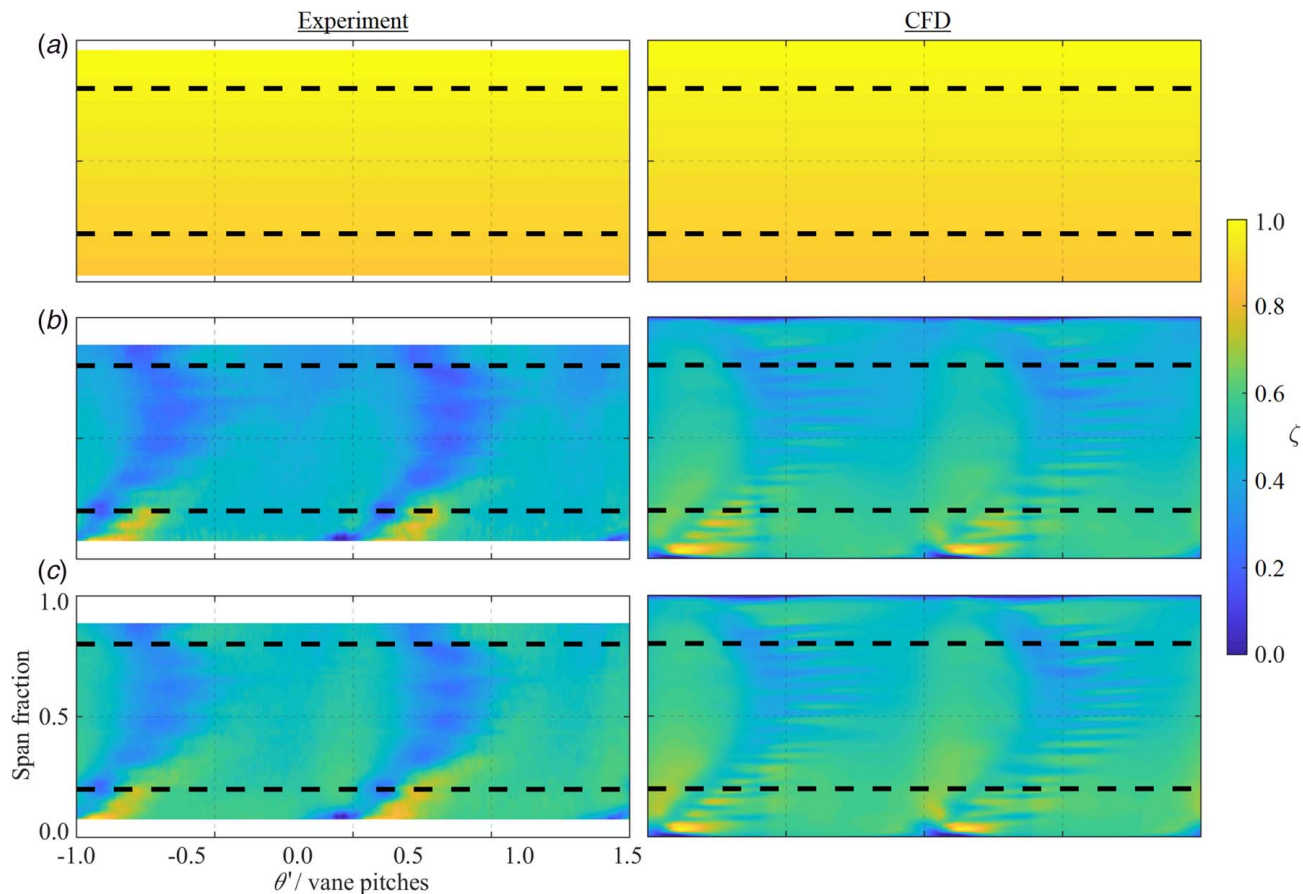


Fig. 8 Experimental and CFD weighting functions in axial plane 1 for (a) area-weighting, (b) volume-flow-weighting, and (c) mass-flow-weighting

normalized static pressure along the wake centerline (red line)—i.e., following one of the dashed white lines in Fig. 11(b)—and in the center of the freestream region (blue line). The trends are periodic and approximately in anti-phase with each other. This effect arises because of the periodic intersection of the wake centerlines (and the freestream centerlines) with the elevated static pressure regions extending axially downstream of each TE. Analysis of the entire flow-field is complicated by the fact that the flow is transonic, but in the region between planes 1 and 3, the flow is almost entirely high-subsonic (predominantly in the range $0.75 < M < 1.00$, but with a small region up to $M = 1.05$ at plane 1).

In subsonic flow, as streamlines enter the elevated pressure region (which extends in the downstream direction, almost perpendicular to the streamlines) they are diffused, and turned toward the axial. As streamlines leave the high-pressure region they are accelerated and turned away from the axial, toward higher whirl angle. The alignment between the wakes and the high-pressure region differs between the three axial planes. In planes 1 and 3, streamlines approximately in the center of the freestream region pass through the high-pressure region and are thus turned toward the axial. In plane 2, streamlines approximately in the center of the wake region pass through the high-pressure region. Therefore between planes 1 and 2, the effect is manifest as a relative *increase* in whirl angle in the freestream regions, and a relative *decrease* in whirl angle in the wake regions (compare Figs. 10(a) and 10(b)), and vice versa between planes 2 and 3. This effect, in combination with the gradual mixing out of circumferential nonuniformity, accounts for the complex development with axial distance of the whirl angle distributions in Fig. 10.

These distributions are important because they significantly impact the weighting functions for different averaging methods.

They also explain the apparently contradictory result that the experiment has greater variation in weighting functions across the plane than CFD (Fig. 9). While CFD is under-mixed with respect to the experiment, and therefore has narrower and deeper wakes, the more extreme variation in axial velocity in experiment—caused by greater whirl angle variation—is the dominant factor in determining the weighting function distributions.

The second interesting effect is that the streamwise pressure gradient, which causes diffusion and acceleration of the wakes (red line in Fig. 12(a)), significantly influences the decay process of the wake profiles. This in turn affects the sensitivities of different weighting methods to axial plane. We characterize the wakes in terms of the maximum value of ζ , which we refer to as ζ_{\max} , and the width of the wake (over which ζ exceeds half of ζ_{\max}), which we refer to as w . These two parameters are plotted in Figs. 12(a) and 12(b), respectively, extracted from both experimental and CFD data at midspan.

Peak loss (Fig. 12(b)) follows a quasi-exponential decay in both experiment and CFD. An offset between the two data arises from the familiar under-prediction of mixing by CFD, leading to higher peak loss along the wake centerline.

Axial trends in the wake width, w (Fig. 12(c)), show a highly variable rate of increase. There is a reasonable correlation between regions of streamwise acceleration identified in Fig. 12(a) ($0.00 < x/C_x < 0.15$, $0.45 < x/C_x < 0.60$, $0.95 < x/C_x < 1.00$) and regions of essentially constant w . That is, acceleration due to the local streamwise pressure gradient thins the wake (disproportional influence on low-momentum fluid) but the effect is in competition with mixing processes which always act to thicken the wake. The corollary is that diffusion acts to thicken the wake, and in regions where dp/dz is positive (where z is streamwise distance), there is significant

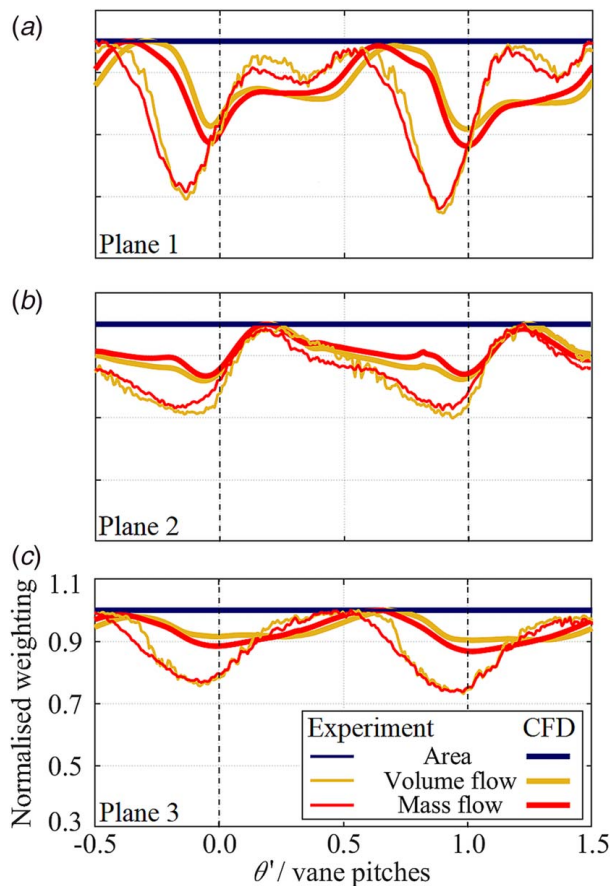


Fig. 9 Normalized midspan weighting functions for each of the three in-plane-averaging methods for experimental and CFD data at (a) Plane 1, (b) Plane 2, and (c) Plane 3. Dashed lines show approximate wake center locations in each plane.

growth in w . In these regions, the effects of diffusion and mixing are additive. A sympathetic impact on the gradient of peak loss might be expected (increase in decay rate where the wake is accelerated, and vice versa), but is hard to discern in the quasi-exponential decay. These results are in accord with Ref. [15], a study of wake flows exposed to different streamwise pressure gradients.

Sensitivity to Radial Averaging Range. To characterize the profile loss, it is necessary to understand the sensitivity to radial averaging range. Mass-flow-weighted ζ is plotted in Fig. 13 as a function of the radial averaging range (expressed as a percentage of vane span, centered on midspan) for both experiment and CFD, and in three axial planes.

For radial averaging ranges between 2 and 10% of span, the returned value of ζ is sensitive to localized spanwise nonuniformities caused by, for example, individual cooling flows or TE slot features. For radial averaging ranges between 10% and approximately 80% of span, the value of ζ is insensitive to local variation, but slowly varying due to nonlinear radial variation in loss coefficient. Near the upper end of this range—say, around 60% of span—may be taken as a sensible radial range for characterizing profile loss. For radial averaging ranges between 80 and 100% of span, the endwall loss becomes more significant, resulting in significant increases in ζ . The depth and breadth of the endwall boundary layers increases with increasing x/C_x . In evaluating ζ for the entire plane (both profile and endwall losses), it is possible to crudely infer the sensitivity to the closeness of approach to the wall (for experimental data) from the near-wall gradient of the trends in Fig. 13.

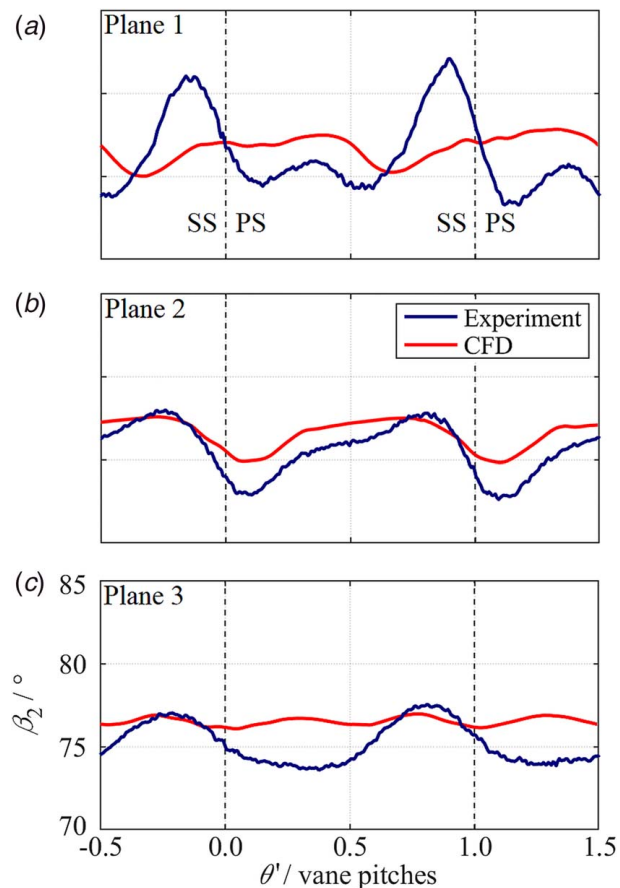


Fig. 10 Circumferential distributions of whirl angle at midspan for experiment and CFD in (a) Plane 1, (b) Plane 2, and (c) Plane 3. Dashed lines show approximate wake center locations in each plane.

Comparison of Plane-Average and Mixed-Out Methods. Plane-average and mixed-out-average results for KE loss coefficient, ζ , are presented for each of the methods discussed, using data from a series of 2D axial planes. The relationships between the trends for total pressure loss coefficient, Y , are almost identical to those for ζ —though they differ in absolute level—and are not presented.

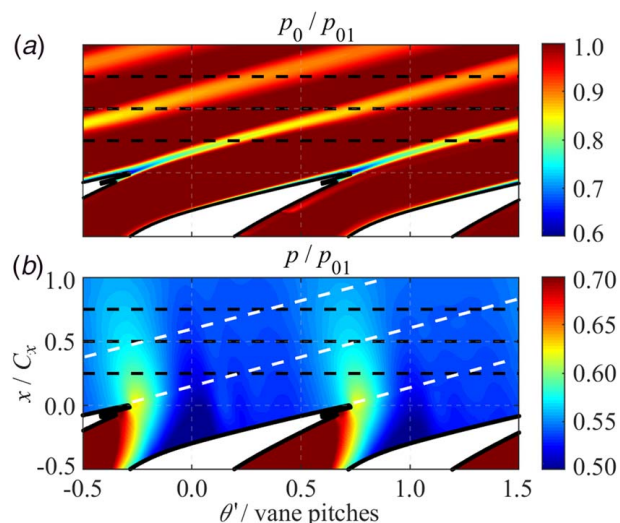


Fig. 11 CFD-predicted midspan contours of (a) normalized total pressure and (b) normalized static pressure

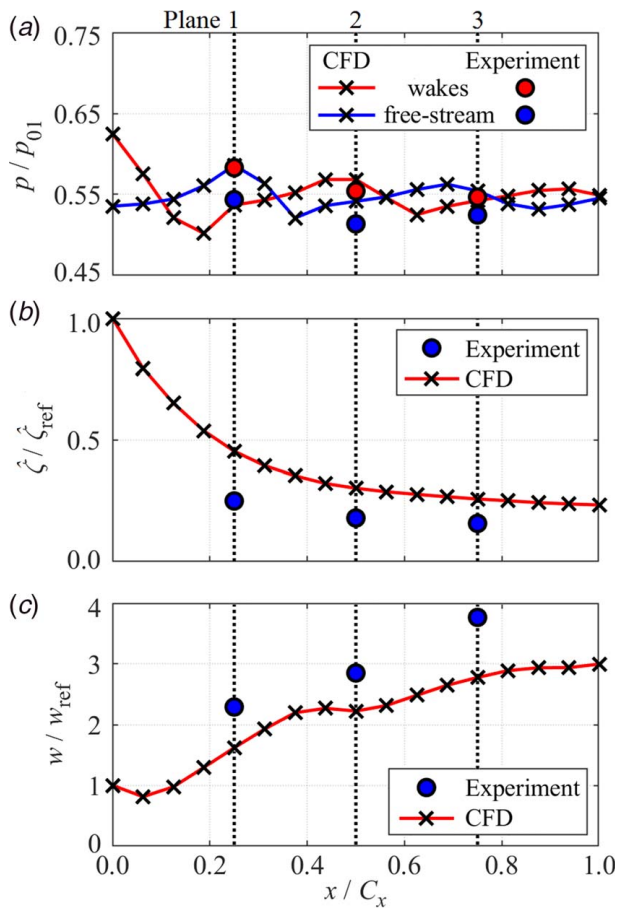


Fig. 12 Axial trends at midspan of (a) static pressure along the wake centerline and in the freestream, (b) peak value of ζ in the wake center, and (c) wake width

Average values of ζ are presented in Fig. 14 as functions of axial location for CFD (16 evenly spaced planes in the range $0 \leq x/C_x \leq 1$) and experiment (traverse planes 1–3 at $x/C_x = 0.25, 0.50$, and 0.75 , respectively). We first compare the trends between experiment and CFD, and conclude the following:

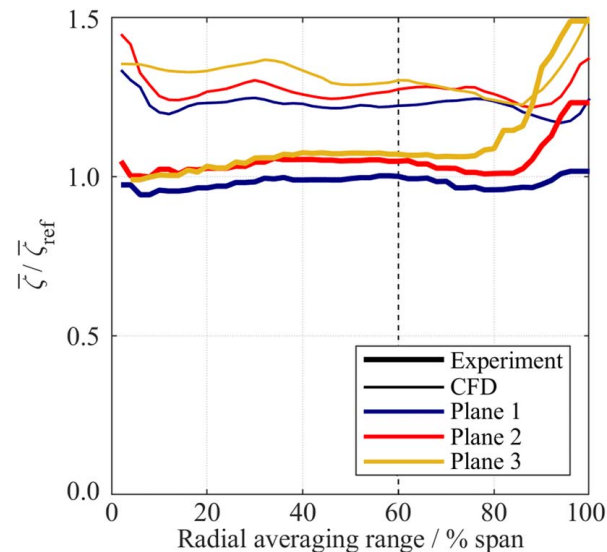


Fig. 13 Mass-flow-weighted average ζ as a function of radial averaging range for experiment and CFD, in three axial planes

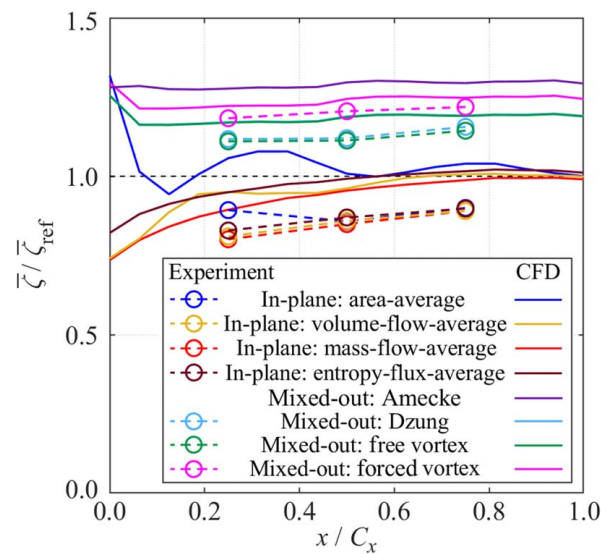


Fig. 14 Axial trends in ζ based on average total pressure according to a number of methods, for experimentally measured and CFD-predicted flows

- (i) There is generally good agreement between the experimental and CFD data, both in terms of absolute level (average difference of +10.0% across all data) and in terms of trends, where the experimental data are in good accord with low-resolution sampling of the corresponding numerical trends. The relative ranking of the in-plane-averaging methods (area-average, volume-flow-average, mass-flow-average, and entropy-flux-average) between experiment and CFD in each of planes 1–3 is similar. In both the experimental and CFD data, the area-average is notably higher than the other three in-plane methods in plane 1, but in closer agreement in planes 2 and 3.
- (ii) The differences in absolute loss between experiment and CFD can generally be attributed to a combination of the CFD being under-mixed; CFD over-predicting the loss associated with surface film cooling; CFD incorrectly predicting the complex TE shock structure and hence the losses associated with shock-boundary layer interaction on the vane suction surface; and inadequate turbulence modeling in the CFD. The differences in the deltas between different averaging methods between experiment and CFD can generally be attributed to the under-prediction of mixing by the CFD. For example, the differences between area-averaged and mass flow-averaged ζ in plane 1 were 10.2% and 18.2% in experiment and CFD, respectively, being smaller in the experimental case because the flow is more fully mixed out in the equivalent axial plane, with less remaining nonuniformity in the wake profile.
- (iii) The average discrepancy in the value of mixed-out KE loss coefficient, ζ , between CFD and experiment (4.3%) is significantly smaller than that in mass-flow-weighted plane-averaged ζ (11.7%), when averaged across all data. On the basis that the CFD is under-mixed with respect to the experiment, this result is initially surprising: one would expect the SKE conversion to loss (difference between in-plane and mixed-out calculations) to be greater for the CFD than the experiment. A possible explanation is provided by Fig. 10, in which we see that the whirl angle variation in the experimental data is great than the CFD data. This provides the experimental data with an additional mechanism for loss generation with axial distance, and may be part of the explanation for this apparently surprising result. Because the agreement is better for mixed-out

coefficients, where absolute comparisons are to be made between experiment and CFD, and where inaccurate prediction of mixing rate is expected (most methods), mixed-out comparisons should be used.

Comparing the different averaging methods, we draw the following key conclusions:

- (i) Trends of in-plane KE loss coefficient, $\bar{\zeta}$, based on volume-flow-averaged, mass-flow-averaged, and entropy-flux-averaged total pressure are for the most part relatively similar to each other: well-behaved, and slowly and monotonically increasing with x/C_x due to the gradual conversion of SKE to total pressure loss. The average (across volume-flow-weighted, mass-flow-weighted, and entropy-flux-weighted trends) change in $\bar{\zeta}$ between $x/C_x=0.00$ and $x/C_x=1.00$ was +23.4% of the latter value. This sensitivity should be considered when choosing an axial traverse plane for flow-averaging or comparing between systems. All of the in-plane methods (including area-weighted average) appear to reach a stable value by $x/C_x=1.00$ and are in agreement in terms of absolute value (to within 2.0%). The absolute convergence of $\bar{\zeta}$ based on the four in-plane total pressure weighting methods is expected, because the variations in the underlying flow-field which give rise to the differences between the weighting functions for the different methods decay rapidly with axial distance (see Fig. 9 and associated analysis).
- (ii) The in-plane KE loss coefficient, $\bar{\zeta}$, based on area-averaged total pressure is *highly* sensitive to axial plane, departing from the other in-plane methods by up to +72.2% (at $x/C_x=0.00$) and varying across the range $0.00 < x/C_x < 1.00$ by between -5.7% and +31.9% of the settled value (at $x/C_x=1.00$). There are numerous problems with the accounting in this method. For example, the significant over-weighting of low-momentum wake regions with respect to other methods (which produces the large peak at $x/C_x=0.00$ where the wake is deepest) and the strong sensitivity to local fluctuations in the wake characteristics (Fig. 12). The simplicity of area-weighted averaging is attractive, but very high sensitivity to axial plane makes it an extremely poor choice for comparisons between CFD and experiment, or between different experiments. In the range $0.00 \leq x/C_x \leq 0.50$, the method should be regarded as unacceptably sensitive to axial location.
- (iii) Volume-flow-weighted averaging of total pressure is more sensitive to axial plane than the mass-flow-average and entropy-flux-average methods, but much less sensitive than the area-average method. The maximum deviation of the volume-flow-average $\bar{\zeta}$ from the mass-flow-average $\bar{\zeta}$ was +8.2%, at $x/C_x=0.19$. Volume-flow-averaging total pressure therefore offers a compromise between achieving a relatively low sensitivity to axial location and practical measurement requirements (does not require measurement of local density variation which may be problematic in some experimental environments).
- (iv) The Dzung and free-vortex mixed-out methods give essentially indistinguishable results for both experimental and CFD data, in accord with the results of Main et al. [8]. The forced-vortex method gives a consistently higher loss with respect to all of the other methods, by an average of +5.8% across all of the data. This difference is attributed to the additional entropy generation associated with producing the required linear radial total pressure distribution. The Amecke method gives the highest loss coefficient of all of the mixed-out methods: and average of +8.8% greater than the Dzung method. The cause of this higher loss is not fully understood.
- (v) All of the mixed-out methods reference a numerically mixed-out flow so—as expected—there is relatively little

sensitivity to axial plane. Between planes 1 and 3 ($0.25 \leq x/C_x \leq 0.75$) the average increases in mixed-out $\bar{\zeta}$ in CFD and experimental data were +1.8% and +3.1%, respectively. Looking more closely at the CFD trend, we see that 85% of the rise in $\bar{\zeta}$ occurs within the range $0.44 < x/C_x < 0.56$, while all of the rise in experiment occurs downstream of plane 2. That is, the wakes passing through an adverse streamwise pressure gradient—i.e., positive dp/dz , where z is streamwise distance (see Fig. 12(a))—causes an increase even in the KE loss evaluated from the mixed-out methods. An adverse pressure gradient increases the velocity gradients in the free shear layers at the wake edges (see discussion related to Fig. 12), and so increases the entropy generation associated with mixing out of the wake profile (rate of entropy generation is proportional to dv/dy , where y is streamwise-normal distance). Conversely, a favorable streamwise pressure gradient (negative dp/dz , where z is streamwise distance) causes a slight reduction in the mixed-out loss. These effects are very small at the operating conditions used in these tests.

Effect of Mach Number. In this section, we use CFD to consider the impact of vane exit Mach number, M_2 , on the applicability of the general conclusions drawn above. We consider five distinct M_2 conditions in the range $0.63 \leq M_2 \leq 1.11$, including the target Mach number ($M_2=0.97$). Absolute values of plane-averaged and mixed-out $\bar{\zeta}$ computed from data at $x/C_x=1.00$ are plotted as functions of M_2 in Fig. 15. The data are normalized with respect to the mean of the four plane-average methods at $M_2=0.97$.

We established previously that at the nominal value $M_2=0.97$, the difference between the four plane-average methods was very small at $x/C_x=1.00$. Figure 15 shows that this result is robust across a wide range of M_2 . In terms of absolute level, all of the mixed-out methods give higher loss coefficient than the in-plane methods. This is due to the mixing out of SKE in the mixed-out methods. The Dzung and free-vortex methods agree almost exactly. The absolute levels of all trends of $\bar{\zeta}$ fall approximately linearly with M_2 in the range $0.63 \leq M_2 \leq 0.97$. We note that this trend is specific to average KE loss coefficient, $\bar{\zeta}$. The equivalent trends (with Mach number) for other performance parameters, e.g., average total pressure loss coefficient, will be different due to their different Mach number sensitivity.

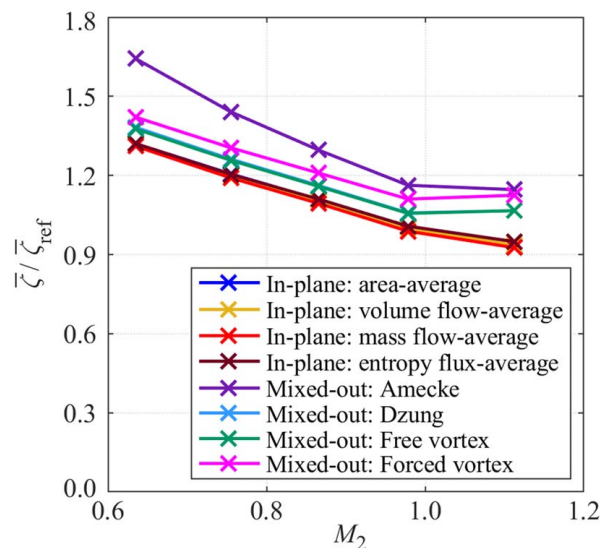


Fig. 15 CFD-predicted plane-average and mixed-out KE loss coefficient, $\bar{\zeta}$, at $x/C_x=1.00$, as functions of vane exit Mach number

In the range $0.97 \leq M_2 \leq 1.11$, plane-average $\bar{\zeta}$ still falls with M_2 , but at a slightly lower rate than at lower M_2 . In contrast, mixed-out $\bar{\zeta}$ increases slightly with increasing M_2 . This suggests a rise in mixing loss at higher M_2 . The additional loss is attributed to the presence of a SS trailing edge shock at $M_2 = 1.11$. There is a small amount of “direct” loss across the shock (total pressure immediately downstream of the shock is slightly lower than that immediately upstream)—this is the cause of the very slight shallowing of the gradient of the in-plane trends in Fig. 15. In poorly resolved CFD, there is smearing-out of the shock, producing an adverse static pressure gradient, which is capable of increasing mixing loss by increasing the rate of shear in regions of velocity gradient. This is a possible cause of the rise in mixed-out KE loss coefficient between $0.97 \leq M_2 \leq 1.11$ in Fig. 15.

We now consider the impact of Mach number on the variation of $\bar{\zeta}$ with axial distance. To do this, we normalize the trends (of the type presented in Fig. 14) by the average value of the four in-plane methods at $x/C_x = 1.00$. The resulting trends with axial distance are shown in Fig. 16 for the two Mach number cases $M_2 = 0.76$ and $M_2 = 1.11$. These data can be compared with those for the design Mach number ($M_2 = 0.97$) shown in Fig. 14. The primary conclusion is that, for a given averaging method, the variation of $\bar{\zeta}$ with axial distance is relatively independent of Mach number. This result is true for all averaging methods. That is, the conclusions drawn from the data of Fig. 14 remain valid across the entire range of typical operating Mach numbers.

For completeness, we note an interesting second-order influence. The axial variation of both the area-weighted and volume-flow-weighted in-plane methods, and mixed-out methods, increases as Mach number is increased. This likely arises because of larger streamwise static pressure gradients (both adverse and favorable) in the flow-field, which amplify the changes in velocity gradient (and therefore changes in entropy generation rate) in the shear layers at the edges of the wakes. The magnitude of the effect discussed in the context of Fig. 12 is therefore increased. Larger

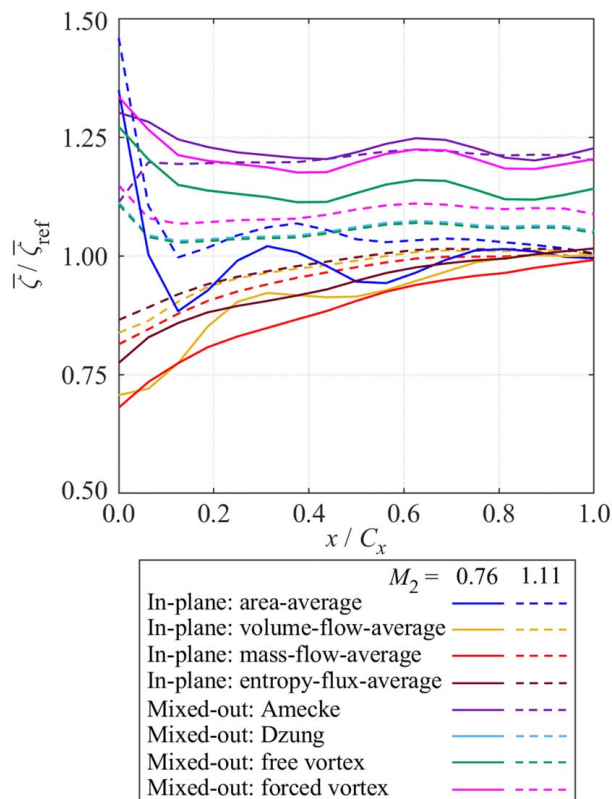


Fig. 16 Variation of $\bar{\zeta}$ with axial distance for two exit Mach numbers: $M_2 = 0.76$ and 1.11

density gradients in the flow at higher Mach numbers also cause a slightly greater difference between the volume-flow-weighted and mass-flow-weighted methods.

Summary and Conclusions

In this paper, we have compared a range of methods for calculating aerodynamic performance parameters—e.g., KE loss coefficient—including plane-average methods with various weighting schemes (area, volume flow, mass flow, entropy-flux) and mixed-out methods in which the flow is artificially mixed to a more uniform state. We do this for the case of a transonic high-pressure (HP) NGV using high-fidelity experimental data from a transonic engine-parts facility, and using complementary CFD. We quantify the sensitivity of the various methods to the axial location of the averaging plane, radial averaging range, and exit Mach number. The underlying physical mechanisms are discussed. The purpose is to provide guidance for a common practical situation on the accuracy of each method when used for comparisons between two or more experiments, or between experiment and CFD.

The key conclusions of this study are as follows:

- (1) The weighting functions for area-weighted, volume-flow-weighted, and mass-flow-weighted plane-averaging methods are strongly influenced by static pressure gradients in the flow. Diffusion and acceleration of the flow cause development of the whirl angle distributions between axial planes and therefore cause changes in the volume flow and mass flow distributions at different planes. The sensitivities reported in this paper will be typical of transonic turbine cascades, but—more generally—the sensitivity to static pressure gradient would be expected to be application-specific.
- (2) The plane-averaged KE loss coefficient based on an area-averaged total pressure is highly sensitive to axial plane, showing variations over the range $0.0 \leq x/C_x \leq 1.0$ of up to -5.7% and $+31.9\%$ of the settled value (at $x/C_x = 1.0$). The axial sensitivity is considered to be unacceptable for measurements made within $0.5 C_x$ of the trailing edge. Despite the simplicity of this method (which makes it a common choice in the literature), the results show that area-averaging is an extremely poor choice for comparing CFD and experiment or comparing different experiments. This conclusion is likely to be valid in most applications with significant wake flow (characterized by low total pressure but also low volume flowrate).
- (3) The plane-average KE loss coefficients based on mass-flow-averaged and entropy-flux-averaged total pressure are very closely matched and have the characteristic of slowly and monotonically increasing with axial distance due to the gradual conversion of SKE to total pressure loss. Plane-average KE loss coefficient based on volume-flow-averaged total pressure is closely matched to the mass-flow-averaged and entropy-flux-averaged methods in terms of both absolute values and axial sensitivity, but shows small differences close to the vane trailing edge due to local density variation. Volume-flow-averaging could be considered to offer a compromise between low axial sensitivity, and practical measurement requirements (does not require measurement of local density variation).
- (4) As expected, mixed-out KE loss coefficients calculated using four different methods are almost independent of axial plane. This is likely to hold true in most applications. Small rises in mixed-out loss coefficient arise when the wakes pass through local streamwise pressure gradients, which increase the velocity gradients (and therefore the rate of entropy generation) in the shear layers at the wake edges. All four mixed-out methods provide closer comparisons between experiment and CFD than the plane-average methods. This highlights the importance of using mixed-out methods for comparing

absolute KE loss coefficient between experiment and CFD, or in situations where inaccurate prediction of mixing rates is expected.

- (5) Mixed-out KE loss coefficients calculated using the Dzung and free-vortex methods were in excellent agreement. Absolute values of mixed-out loss coefficient calculated from the Amecke and forced-vortex methods were higher than the first two methods. If a single method is to be chosen, the Dzung method might be preferred due to its ease of implementation and unproblematic inclusion of coolant flows.
- (6) The axial sensitivity of KE loss coefficient is relatively independent of Mach number—a result that holds true for all plane-average and mixed-out methods. At higher Mach number, the associated larger density gradients in the flow slightly increase the axial variation in both plane-average and mixed-out loss coefficients.
- (7) For the NGV studied, radially averaging over the central 60% of vane span is robust for characterizing profile loss. This range is sufficiently large to avoid sensitivities due to local radial nonuniformities (particular cooling features, etc.) but not so large as to include sensitivity to endwall flows, which is often problematic where comparisons between situations (e.g., CFD and experiment) are required.

Acknowledgment

The support of Rolls-Royce plc and Innovate UK are gratefully acknowledged.

Data Availability Statement

The authors attest that all data for this study are included in the paper.

Nomenclature

h = static enthalpy, J/kg
 p = static pressure, Pa
 r = radial position, m
 s = static entropy, J/(kg K)
 v = velocity, m/s
 w = wake width, m
 x = axial distance or direction, m
 y = streamwise-normal distance, m
 z = streamwise distance, m
 A = area, m²
 M = Mach number, dimensionless
 Y = stagnation pressure loss coefficient, dimensionless
 \dot{m} = mass flowrate, kg/s
 \dot{q} = volume flowrate, m³/s
 c_p = specific heat at constant pressure, J/(kg K)
 h_0 = stagnation enthalpy, J/kg
 p_0 = stagnation pressure, Pa
 p_{ref} = arbitrary reference pressure, Pa
 r_1 = lower radial bound for integration, m
 r_2 = upper radial bound for integration, m
 v_x = axial velocity component, m/s
 w_{ref} = reference wake width at $x/C_x = 0.0$, m
 C_x = axial chord length, m
 M_2 = vane exit Mach number, dimensionless
 T_0 = stagnation temperature, K
 $\overline{p_{02}}$ = mean total pressure in a downstream plane, Pa
 $\overline{p_2}$ = mean static pressure in a downstream plane, Pa
 Re = Reynolds number, dimensionless
 Tu = turbulence intensity, %

Greek Symbols

β = flow turning (or whirl) angle, deg
 γ = ratio of specific heats, dimensionless
 ζ = kinetic energy loss coefficient, dimensionless
 $\hat{\zeta}$ = maximum kinetic energy loss coefficient, dimensionless
 $\hat{\zeta}_{\text{ref}}$ = reference maximum kinetic energy loss coefficient at $x/C_x = 0.0$, dimensionless
 $\bar{\zeta}$ = average kinetic energy loss coefficient, dimensionless
 $\bar{\zeta}_{\text{ref}}$ = reference average kinetic energy loss coefficient (mean of plane-average methods at $x/C_x = 1.0$), dimensionless
 η = isentropic efficiency, dimensionless
 θ = circumferential position, deg
 θ' = normalized circumferential position, vane pitches
 θ_1 = lower circumferential bound for integration, deg
 θ_2 = upper circumferential bound for integration, deg
 ρ = mass density, kg/m³
 $\chi = (\gamma - 1)/\gamma$

Subscripts

0 = stagnation condition
 1 = vane inlet station
 2 = vane exit station
 A = area-weighted average value
 M = mass-flow-weighted average value
 s = isentropic condition
 S = entropy-flux-weighted average value
 V = volume-flow-weighted average value

References

- [1] Dzung, L. S., 1971, "Konsistente Mittelwerte in der Theorie der Turbomaschinen für Kompressible Medien," *BBC-Mitt.*, **58**, pp. 485–492.
- [2] Amecke, J., 1970, "Anwendung der Transsonischen Ähnlichkeitsregel auf die Strömung Durch Ebene Schaufelgitter," *VDI-Forschungsheft*, **540**, pp. 16–28.
- [3] Pianko, M., and Wazelt, F., 1982, "Propulsion and Energetics Panel Working Group 14 on Suitable Averaging Techniques in Non-Uniform Internal Flows," AGARD Advisory Report No. 182. NATO Advisory Group for Aerospace Research and Development, Neuilly-sur-Seine, France.
- [4] Oates, G. C., 1997, *Aerodynamics of Gas Turbine and Rocket Propulsion*, AIAA, Reston, VA, pp. 197–203.
- [5] Cumpsty, N. A., and Horlock, J. H., 2005, "Averaging Non-Uniform Flow for a Porpoise," Proceedings of ASME Turbo Expo 2005, Reno-Tahoe, NV, June 6–9.
- [6] Denton, J. D., 1993, "The 1993 IGTI Scholar Lecture: Loss Mechanisms in Turbomachines," *ASME J. Turbomach.*, **115**(4), pp. 621–656.
- [7] Greitzer, E. M., Tan, C. S., and Graf, M. B., 2004, *Internal Flow: Concepts and Applications*, Cambridge University Press, Cambridge, UK.
- [8] Main, A. J., Oldfield, M. L. G., Lock, G. D., and Jones, T. V., 1997, "Free Vortex Theory for Efficiency Calculations From Annular Cascade Data," *ASME J. Turbomach.*, **119**(2), pp. 247–255.
- [9] Prasad, A., 2005, "Calculation of the Mixed-Out State in Turbomachine Flows," *ASME J. Turbomach.*, **127**(3), pp. 564–572.
- [10] Dominy, R. G., and Harding, S. C., 1989, "An Investigation of Secondary Flows in Nozzle Guide Vanes," Proceedings of AGARD PEP 74th Secondary Flows in Turbomachines, Luxembourg, Aug. 28–Sept. 1, Paper No. AGARD-CP-469.
- [11] Kirolos, B., Lubbock, R., Beard, P., Goenaga, F., Rawlinson, A., Janke, E., and Povey, T., 2017, "ECAT: An Engine Component Aerothermal Facility at the University of Oxford," Proceedings of ASME Turbo Expo 2017, Charlotte, NC, June 26–30, Paper No. GT2017-64736.
- [12] Povey, T., Sharpe, M., and Rawlinson, A., 2011, "Experimental Measurements of Gas Turbine Flow Capacity Using a Novel Transient Technique," *ASME J. Turbomach.*, **133**(1), p. 011005.
- [13] Burdett, D., Hambidge, C., and Povey, T., 2021, "Analysis of Ultra-Low Uncertainty Gas Turbine Flow Capacity Measurement Techniques," *Proc. Inst. Mech. Eng. Part A: J. Power Energy*, **235**(5), pp. 1053–1079.
- [14] Burdett, D., Goenaga, F., and Povey, T., 2021, "Understanding Capacity Sensitivity of Cooled Transonic Nozzle Guide Vanes," *ASME J. Turbomach.*, **143**(5), p. 051001.
- [15] Thomas, F. O., and Liu, X., 2004, "An Experimental Investigation of Symmetric and Asymmetric Turbulent Wake Development in Pressure Gradient," *Phys. Fluids*, **16**(5), pp. 1725–1745.